

We are IntechOpen, the world's leading publisher of Open Access books Built by scientists, for scientists

6,900

Open access books available

186,000

International authors and editors

200M

Downloads

Our authors are among the

154

Countries delivered to

TOP 1%

most cited scientists

12.2%

Contributors from top 500 universities



WEB OF SCIENCE™

Selection of our books indexed in the Book Citation Index
in Web of Science™ Core Collection (BKCI)

Interested in publishing with us?
Contact book.department@intechopen.com

Numbers displayed above are based on latest data collected.
For more information visit www.intechopen.com



Scaling Laws in Low-Speed Switched Reluctance Machines

Pedro Lobato, Joaquim A. Dente and Armando J. Pires

Abstract

In low-speed applications, switched reluctance machine (SRM) design methodologies are generally driven by criteria related to the number of pole pair combinations in the stator and rotor of regular machines. In this chapter, a set of scaling laws are developed in order to compare magnetic topologies of regular and non-regular machines. Through the introduction of constraints, the proposed methodology integrates thermal and magnetic saturation phenomena. Within a selected set of short flux-path topologies and using finite element analysis, it is possible to verify which topology is the most appropriate. As an illustrative application, the chosen topology—a modular one—is compared with a regular prototype of a switched reluctance generator designed for a wind energy turbine by using a linear model in conjunction with the scaling laws. The evaluation of the two topologies shows the significant increase of power per unit of mass and lower losses of the modular topology than the regular one. The application of scale model methodology is extensive to the design of higher-speed machines. Valuing the dimensional and similarity arguments, certain assumptions of the machine design gain a special emphasis in this work, bringing the discussion of these machines to another paradigm.

Keywords: machine design, scale model methodology, similarity laws, low-speed energy converters, switched reluctance machine

1. Introduction

Over the last decades, various technical aspects such as design, modelling, analysis, and control of switched reluctance machines (SRM), turned research attention to further improvements in the machine operation. Topics of investigation, including control techniques, loss optimization, torque ripple, and acoustic noise, illustrate the progress in knowledge of motoring mode operation.

The SRM behaves, intrinsically, as a variable speed drive that can be controlled, according to the load, through the energizing and de-energizing moments of the stator phases [1]. Robustness and simple construction (stator-concentrated windings only), control flexibility, and high tolerance over a high-speed range [2] are attributes that qualify it even for the harshest environments [3]. Short flux-path topologies make use of design techniques that facilitate maintenance and improve the machine performance.

The motor operation of this machine has often been the target of research, in detriment of the generator operation. The switched reluctance generator (SRG)

research has been primarily focused on high-speed application design [4]. In these cases, the magnetic topologies are generally of the regular type [5], with two poles diametrically opposed in each stator winding phase and a minimum number of rotor poles. The applications of the SRM as a SRG are in the fields of aerospace, automotive, and wind energy [6].

Research work has been published, for more than a decade, on the application of SRG to wind power systems. Despite the efforts and different possibilities of designing the magnetic circuit of the SRG, regular topologies are usually presented for this type of applications, with an appropriate combination of stator and rotor poles [7]. The laws of scale, also called laws of similarity [8], formulated here, are a useful tool to compare magnetic topologies. This proposed scale model methodology allows to evaluate the effect of thermal phenomena and magnetic saturation of the materials that constitute the electrical and magnetic circuits of the machine. The scale relationships that are established between these circuits differ from topology to topology, by the specific characteristics of these circuits and the relative position they occupy in the structure of the machine.

Thus, in this work, dimensional and symmetry arguments are invoked in the choice of magnetic topologies, leading the discussion about the SRG project to another paradigm.

In the field of renewable energy conversion, high-torque and low-speed machines have gained market space, namely, in wind power applications. The trend towards offshore resource exploitation and consequently the increasing capacity of wind turbines impose robust and reliable solutions, which are critical attributes for wind generators, for an economically and environmentally sustainable operation. In this sense, gearboxes are a component of the system to be avoided in system design, because of the high weight, cost, and unpredictable lifetime.

These are the main reasons that manufacturers in conjunction with research teams have been pursuing direct drive wind energy systems, where the permanent magnet synchronous generator (PMSG) stands out. However, the fluctuating cost of the neodymium (NdFeB), constituting the magnets, has raised some reservations on the consensus opinion about these generators [9]. In addition, harsh on-site installation and operation conditions require special attention to thermal and mechanical stresses; otherwise they will degauss and reduce overall system performance [10]. At this delicate issue, the SRM presents itself as a simple, robust, and cost-effective structure as it does not require permanent magnets or rotor windings. Combined with control flexibility, high reliability, and fault tolerance, it makes this machine attractive for direct drive energy converters (**Figure 1**).

The remainder of this chapter is organized as follows: Section 2 examines some design issues and proposes similarity laws for a SRG design methodology. Section 3

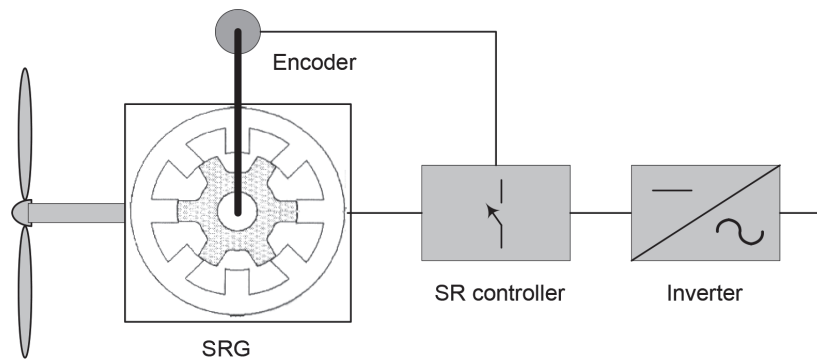


Figure 1. Schematic representation of a SRG applied to a direct drive wind energy converter (the stator structure is shown without the coils, for an easier understanding).

discusses the features of short-flux path magnetic topologies, using finite element analysis, and a linear field-based model is proposed. Section 4 presents results from the comparison of a modular short-flux path topology, with a 20 kW regular SRG prototype operating at a rated speed in the region of 100 rpm, for use in a direct drive wind turbine [11]. Finally, Section 5 offers some conclusions and points out some impacts of the scale model methodology in the design procedure.

The work presented in this chapter introduces a simple and already known dimensional similarity-based methodology, built however on another paradigm, ready to be used as a design tool for estimation of SRG characteristics and comparison of SRM topologies.

2. Formulation of similarity laws

The SRM design flexibility is consistent with a large number of poles, and there are various magnetic topologies that can support low-speed applications. In spite of that diversity of feasible topologies, there are some intrinsic constraints affecting their dimensions and performance. The characterization and differentiation of constraints are considered priorities in order to adopt a suitable methodology to help in the selection of the magnetic topology and geometry for each application. A constraint can be distinguished by its nature, physical and material. Since the operation of the SRM is sustained by the magnetic field, a first type of constraints can be a result of the physical phenomena involved in the electromagnetic conversion. A second type of constraints emerges from the domain of the material properties, depending on the limits of insulators and magnetic materials used. As examples, the practical constraint of fixing the flux density results from the saturation limit inherent to the magnetic material, or fixing the temperature limits prevents premature deterioration of insulators and the shortening of the equipment lifetime. Additionally, variables such as power, losses, and weight should be taken into consideration as they also play an important role in the machine design and construction. The estimation of certain characteristics of the machine can be facilitated by the relationship between these variables. Models based on similarity laws were chosen, bearing in mind a machine design oriented towards a change of scale.

2.1 Rated power and losses

In the machines based on magnetic field properties, the displacement current term in Maxwell's equations can be neglected, taking into account the frequencies and sizes involved. By neglecting this term, Maxwell's equations will be in the magneto-quasi-static form. There is a physical constraint due to the electromagnetic linkage of electrical and magnetic circuits in both cases, the motoring and the generating mode operations. This linkage is represented in Eq. (1), where an implicit relationship of characteristic dimensions for each type of circuit is also shown:

$$\text{rot } H = J \quad (1)$$

Considering a change of scale in the construction-oriented machine design, Eq. (1) can be written in the form of (2), where l represents a characteristic linear dimension:

$$B \propto J l \quad (2)$$

This proportional relationship highlights that magnetic circuits, excited by a current, impose a scale factor in their linear dimensions, which is echoed in the relationship B/J . Therefore, by modifying that characteristic linear dimension, important changes of performance and machine features can be achieved.

Other variables, like power, losses, and material weight, are also critical in the machine design. So, it is important to find the scale relationships involving some of the mentioned variables and the machine dimensions, with the purpose of comparing and predicting certain SRG dimensional characteristics and parameters, based on scale models.

For that aim, the understanding of the energy conversion principles of the SRM is a first step and can be easily described using the generating mode operation, represented in **Figure 2**.

Neglecting saturation phenomena at this point, **Figure 2** shows the profiles of idealized inductance L , phase flux-linkage ψ , phase current i , and voltage u for a SRG for single-pulse operation, where V_S is the dc-link voltage and L_a and L_{na} are, respectively, the aligned and unaligned inductances. In a regular SRM, with N_R rotor poles, those waveforms are periodic in τ_R , which is the rotor pole pitch ($2\pi/N_R$). During the excitation period, from the rotor position θ_{on} to θ_{off} , energy is stored in the machine magnetic field, with the current supplied by the electrical source. After commutation, at θ_{off} , the excitation energy is returned to the source, and simultaneously, the energy provided by the prime mover is converted to electrical energy.

At θ_e , all the flux from excitation period is extinguish, and no more electrical energy is returned to the source. Neglecting the losses, the output energy over each stroke exceeds the excitation energy by the mechanical energy supplied.

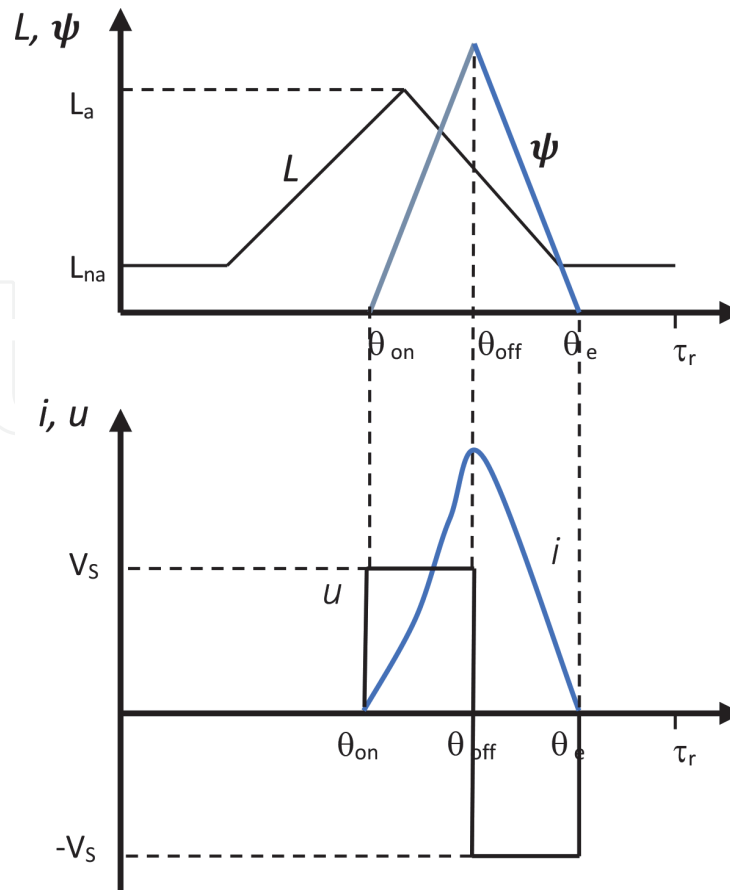


Figure 2.
Idealized inductance profile and waveforms of a single-pulse controlled SRG.

The SRM can operate continuously as a generator, if the electrical output energy exceeds the excitation energy, i.e., maintaining the excitation period so that the bulk of the winding conduction period comes after the aligned position ($dL/d\theta < 0$). It is considered that the SRG can operate in single-pulse mode, at all speeds, which results in low switching losses.

To better clarify the issues related to the excitation of the SRG and to extract energy from the phase winding, it is useful to look at the electrical equations of an SRG phase as follows:

$$u = \frac{d\psi}{dt} + Ri \tag{3}$$

Multiplying both members of Eq. (3) with the phase current, neglecting the ohmic losses and assuming a non-saturated machine ($\psi = L(\theta)i$), the instantaneous power is given as

$$ui \cong i \frac{d\psi}{dt} \cong iL \frac{di}{dt} + i^2 \frac{dL}{d\theta} \omega \tag{4}$$

where ω is the angular speed of the rotor ($\omega = d\theta/dt$).

The SRM energy converter can be represented as a lossless magnetic energy storage system, with electrical and mechanical terminals, as shown in **Figure 3**. In this type of system, the magnetic field serves as the coupling channel between the electric and mechanical terminals. This kind of representation is valid in situations where the loss aspects can be separated from the storage aspects and is also useful in generating mode operation, where the average torque is negative.

For the lossless magnetic energy storage system, the instantaneous power flow in the system can be expressed by

$$ui = \frac{dW_m}{dt} + T_e \omega \tag{5}$$

where W_m is the stored energy in the magnetic field expressed by (6) and T_e is the electromagnetic torque. For a linear system, the magnetic energy W_m and coenergy W_c are numerically equal. Thus, the time rate of the magnetic energy change is given by (7), and T_e can be obtained from the coenergy as indicated in (8):

$$W_m = \frac{1}{2} Li^2 \tag{6}$$

$$\frac{dW_m}{dt} = iL \frac{di}{dt} + \frac{1}{2} i^2 \frac{dL}{d\theta} \omega \tag{7}$$

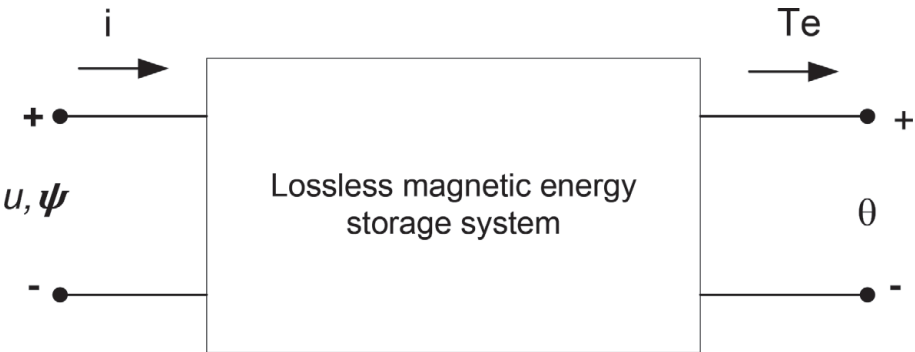


Figure 3.
Schematic magnetic field-based SRM energy converter.

$$T_e = \frac{\partial W_c}{\partial \theta} = \frac{1}{2} i^2 \frac{dL}{d\theta} \quad (8)$$

After replacing T_e in Eq. (5), comparing it with Eq. (4) allows to conclude that less than half of the electrical power involved in the system is converted from the mechanical power of the prime mover. In fact, part of it is being stored in the magnetic field. It should be noted that this conclusion has been established in terms of instantaneous power and for a non-saturated machine. However, for scaling design, based on similarity laws, the average power and the torque are considered fundamental. The average power $\langle p \rangle$ is given by (9), where the rotor angular speed is considered constant. Both current and phase inductance can be written as functions of the rotor position and the maximum values, I and L_a , respectively, as represented in Eqs. (10) and (11). Multiplying these functions, the phase flux-linkage is represented by (12). Thus the average power per phase, expressed in (9), is transformed in by (13), in such way that the integral $\int_0^{\tau_r} \xi_{(\theta)}^2 \frac{d\chi_{(\theta)}}{d\theta} d\theta$ should result in a constant value.

$$\langle p \rangle = \langle ui \rangle = \langle T_e \rangle \omega \quad (9)$$

$$i = I \cdot \xi_{(\theta)} \quad (10)$$

$$L = L_a \cdot \chi_{(\theta)} \quad (11)$$

$$\psi = Li = L_a I \cdot \xi_{(\theta)} \chi_{(\theta)} \quad (12)$$

$$\langle p \rangle = \frac{\omega}{2\tau_r} \int_0^{\tau_r} i^2 \frac{dL}{d\theta} d\theta = \frac{\omega}{2\tau_r} I^2 L_a \int_0^{\tau_r} \xi_{(\theta)}^2 \frac{d\chi_{(\theta)}}{d\theta} d\theta \quad (13)$$

Considering the dimensional analysis, the similarity laws for ψ , I , and L_a can be expressed by (14), (15), and (16), where the scale factor naturally takes place. Having in mind Eq. (13), a proportional relationship for $\langle p \rangle$ can be written as (17):

$$\psi \propto Bl^2 \quad (14)$$

$$I \propto Jl^2 \quad (15)$$

$$L_a \propto \frac{\psi}{I} \propto \frac{B}{J} \quad (16)$$

$$\langle p \rangle \propto N_R \omega (Jl^2)^2 \frac{B}{J} \propto N_R \omega B J l^4 \quad (17)$$

Considering an m -phase SRM, and in terms of similarity laws, the rated power can be expressed by (18)

$$P \propto m N_R \omega B J l^4 \quad (18)$$

Identical similarity laws can be written for motor mode since the physical fundamental concepts are similar. It should also be highlighted that the criteria of selecting the number of variables, greater or smaller, to be explicit in the scale laws, depend only on the parameters and characteristics considered relevant for the comparison of topologies that is proposed. For instance, the number of rotor poles is a significant parameter in evaluating low-speed SRG designs, since J should be kept under certain limits due to copper losses and the preservation of the insulating material and B is limited by magnetic saturation of the iron. The influence of the commutation of phases on the torque, for this dimensional analysis, was neglected.

In fact, assuming similar levels of saturation (of B), it is assured that the abovementioned comparison of topologies, in relative terms, is valid. Therefore, a compromise involving the number of poles, the dimensions related with both the magnetic and electrical circuits, and the phase current is required. For that purpose, particular design details of SRM topologies related with the magnetic circuit drawing and the windings location will be investigated, in order to increase the available inner space of the machine, taking advantage of an improved air circulation. These aspects will be addressed in Section 3.

2.2 Multi-machine topology

Regarding to SRM design, there is a high number of feasible topologies, which are differentiated by the properties of the electrical and magnetic circuits, and their relative location. A possible SRG topology for an energy converter can include a series of n -SRM assembled on a common axis. The mono-axial multi-machine topology presents a higher fault tolerance and a simpler maintenance, compared with a monolithic SRM.

The previous relationships, applied in SRG design, are suitable to observe certain limitations and some effects of the scale laws. The methodology will be applied considering a SRG that is characterized by the rated power, the copper and iron losses, the maximum value of flux and the current densities, the temperature, and the efficiency. These values are assumed as reference values, allowing the comparison with similar machines, but built in a different scale.

In the methodology of scale models, applied to an electromagnetic device, there is one freedom degree to select the variables B and J as both are interconnected by (2). The saturation levels should be kept constant in all regions of the magnetic circuit, although the flux density is significantly different depending on the regions and instants. Therefore, the practical limitation imposed by the saturation of the magnetic materials can be expressed, in terms of scale laws, by (19):

$$J \propto \frac{B}{l} \quad (19)$$

According to scale laws, it is possible to compare the relative losses of a hypothetical SRG topology, composed of a set of n machines assembled in the same shaft, with a similar monolithic SRG, even though much larger but with the same rated power of the previous one. Assuming a constant rotor speed and equal number of phases and rotor poles of both topologies, the scale law for rated power P_N can be rewritten simply by

$$P_N \propto B^2 l^3 \quad (20)$$

For one SRM module of the multi-machine topology, the rated power can be expressed by

$$P_m \propto B_m^2 l_m^3 \propto B^2 l_m^3 \quad (21)$$

where B and B_m are the flux densities, considered equal once both topologies use the same core material, and l_m is a linear dimension of the multi-modular topology. However, this multi-modular topology is characterized by the total rated power shared by n SRM modules as follows:

$$P_m = \frac{P_N}{n} \quad (22)$$

Moreover, for comparison purposes of topologies, one searches a relation that involves linear dimensions of both topologies and number of modules. Using (20), (21), and (22), a scale law can be expressed by

$$\frac{l_m}{l} \propto \left(\frac{1}{n}\right)^{1/3} \quad (23)$$

This result states, as expected, that as the number of modules is higher, smaller will be the relative linear dimension. Using the previous proportionality law, a relationship that allows the comparison of the relative copper losses in both topologies can be established:

$$\frac{P_{JmT}}{P_J} \propto \frac{nmJ_m^2 l_m^3}{mJ^2 l^3} \propto n \left(\frac{l_m}{l}\right) \propto n^{2/3} \quad (24)$$

Using (23) and (24) the scale law concerning the relative copper losses can be expressed by (25) and represented in **Figure 4**, with the condition of having a constant flux density:

$$p_{jr} \propto \frac{P_{JmT}}{P_N} \propto n^{2/3} P_N^{-2/3} \quad (25)$$

So, regarding copper losses, it is possible to conclude about a scale gain for larger monolithic SRM, rather than a modular system composed by SRM units. However, the multi-machine topology could be elected for certain applications where other aspects are a priority like fault tolerance, low cost, and easy maintenance.

2.2.1 Constraint imposed by temperature

In the machine design, at some stage, the heating phenomena have to be considered. In effect, the compromise settled the temperature increase, and the proper temperature levels of insulating materials are critical in the machine lifetime. In order to obtain a scale law, under the thermal stability conditions, it is assumed that the temperature variation $\Delta\theta$ can be expressed by (26). It is introduced h_e as the

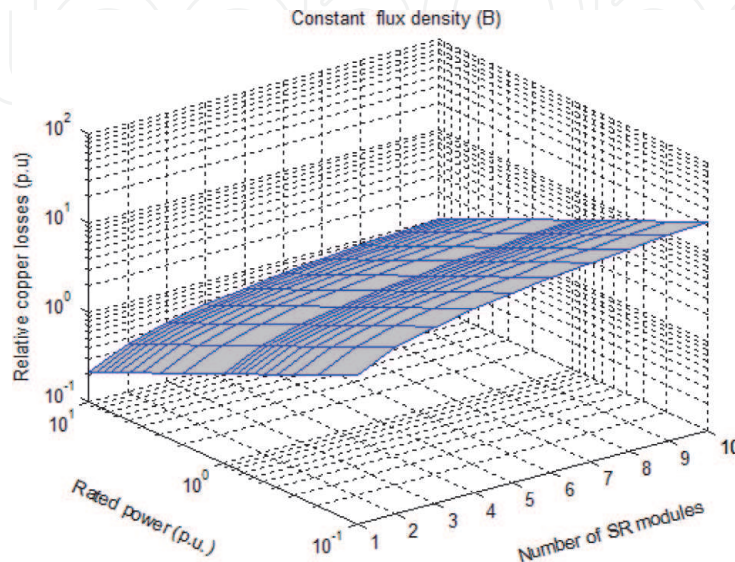


Figure 4.
Relative copper losses for scale models of SRM considering magnetic saturation constraint.

equivalent heat transfer coefficient for all heat exchanges between a fluid and a solid, where A_S is the area of the boundary surface of the material:

$$\Delta\vartheta \propto \frac{P_J}{h_e A_S} \propto \frac{mJ^2 l^3}{l^2} \propto J^2 l \quad (26)$$

Once the constraint of temperature as an influential criterion for comparison purposes is introduced, the current density is expressed by (27), which points out the lower current density in larger machines:

$$J \propto \frac{1}{\sqrt{l}} \quad (27)$$

Therefore, the former scale relationship indicated for rated power (28), and the relationship between linear dimensions (23), is replaced respectively by (28) and (29):

$$P_N \propto m N_R \omega l^4 \quad (28)$$

$$\frac{l_m}{l} \propto \left(\frac{1}{n}\right)^{1/4} \quad (29)$$

Taking into account these two relationships and following the steps presented in Subsection 2.2, the relative copper losses in such temperature conditions are ruled by the scale laws (30) and (31). **Figure 5A** shows the behavior of those losses considering the rated power of the reference machine and the number of modules:

$$\frac{P_{JmT}}{P_J} \propto n^{1/2} \quad (30)$$

$$P_{Jr} = \frac{P_{JmT}}{P_N} \propto n^{1/2} P_N^{-1/2} \quad (31)$$

It is observed that the scale gain effect persists for larger monolithic SRM systems, rather than multi-machine systems, despite the temperature constraint and due to lower relative losses in the previous case. Indeed, the relative copper losses are smaller for larger machines and higher for smaller machines due to the current density, which assume, in relative terms, smaller values in large SRM, as shown in **Figure 5B**. This dimensional analysis makes possible to forecast that the efficiency tends to increase in large SRM systems and decrease in small ones. To counteract that trend in smaller machines, it is considered a good practice to increase, in relative terms, the linear dimension of the copper and decrease the dimension of the magnetic circuit.

From **Figure 5B** it can be inferred that for larger machines it is easy to drive into saturation once the flux density can achieve higher levels. Unlike the smaller machines design, in larger machines emphasis should be placed on the circuit magnetic dimension combined with the decrease of the relative dimension of the conductive material. These results suggest a split of scales, thereby benefiting from the behaviors of B and J with regard to the rated power. That split of scales reflects in practice by making use of two distinct scales, one for copper and another for iron. Next steps of the scale analysis will follow in that direction.

2.2.2 Differentiated scales for copper and iron

Until now, the design study has been based on a geometrical scale factor with additional constraints to fix B and J densities. It becomes clear, from the last results,

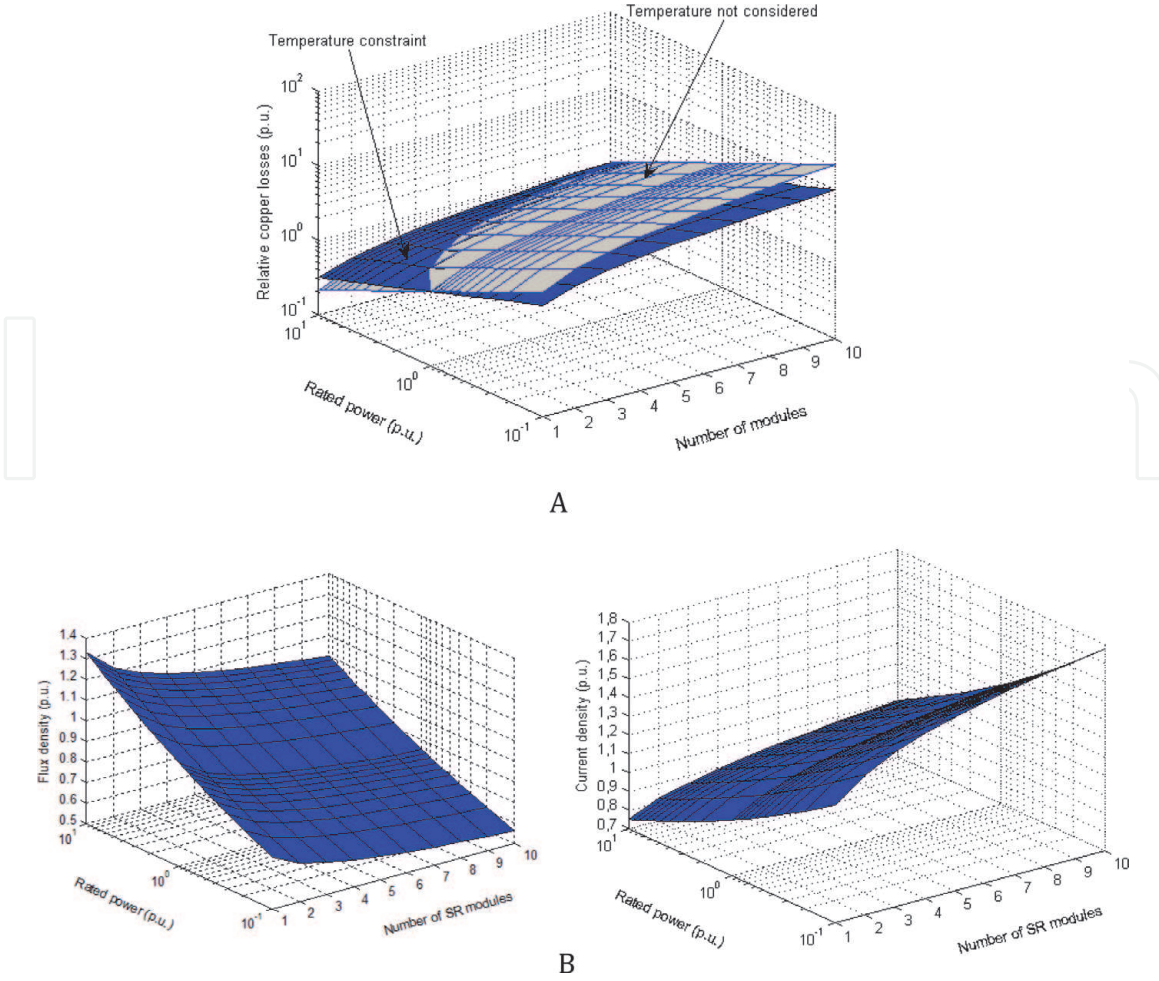


Figure 5. (A) Relative copper losses for scale models of SRM considering temperature constraint. (B) Normalized current density and flux density for scale models of SRM considering temperature constraint.

that a degradation of the overall system efficiency, when the SRG is composed of several SRM units, is expected. In fact, the adoption of the scale criteria has shown an increase of modules current density, which in turn causes higher copper losses. This increase of copper losses is not balanced by the flux density decrease.

Trying to improve the use of the conductive material and the core iron, it is of interest to introduce a modification into the linear scales. This option is accomplished through a structural change, in which two specific dimensions of each material will be used, I_{Cu} and I_F . Therefore, the relationship (18) assumes the form of (32), and the relationship (2) is rewritten as (33). These two degrees of freedom correspond to an equal number of constraints in order to fix the flux and current densities:

$$P_N \propto m N_R \omega (B l_F^2) (J l_{Cu}^2) \quad (32)$$

$$B l_F \propto J l_{Cu}^2 \quad (33)$$

Taking as reference the regular monolithic machine, each SRM unit provides only a part of the rated power and enables to infer a new relationship between the relative dimensions of the SRM and the number of modules.

The two available degrees of freedom are used to keep the density flux, as well as the temperature variation as a constant. In such case, the copper characteristic dimension plays a key role in limiting the temperature increase. The relationship (27) will be replaced by (34):

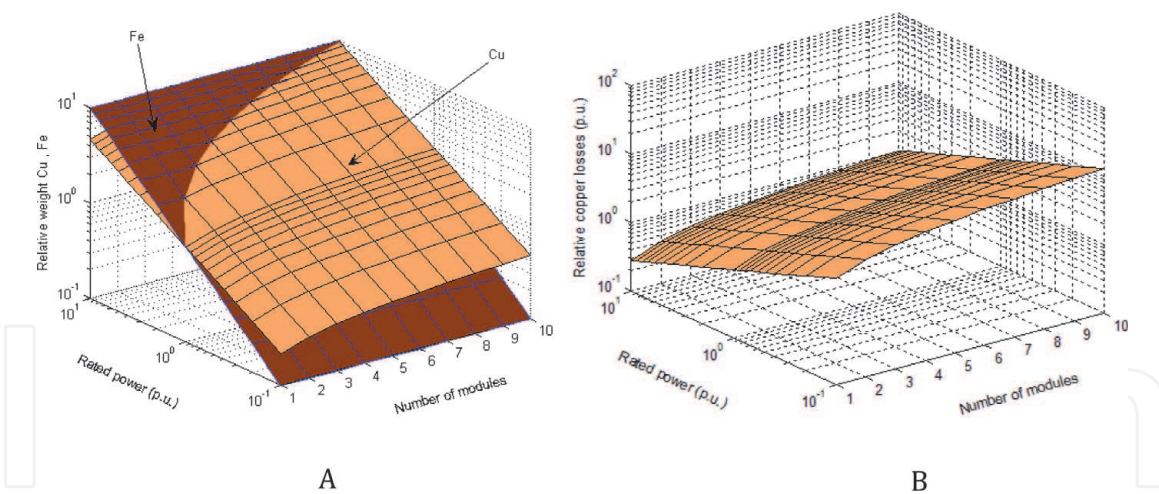


Figure 6.
 (A) Relative weights of iron and copper, keeping flux density and temperature increase both constant.
 (B) Relative copper losses with temperature increase and density flux both constant.

$$J \propto \frac{1}{\sqrt{I_{Cu}}} \quad (34)$$

The materials weight is proportional to the cube of the respective specific dimensions. So, the relationships (35) and (36) are considered representative of the copper and iron weights of the modules set, $Wt_{F_{mT}}$ and $Wt_{Cu_{mT}}$.

Observing **Figure 6A** it can be highlighted that the copper weight increases with the number of modules and decreases with the rated power, in relative terms. The iron weight is proportional directly to the rated power and is independent from the number of SRM modules:

$$Wt_{F_{mT}} \propto P_N \quad (35)$$

$$Wt_{Cu_{mT}} \propto n^{1/3} P_N^{2/3} \quad (36)$$

The variation of temperature, within a restricted range, and the constant flux density lies on preventing the limits of temperature and the materials magnetic saturation to be exceeded. Under these constraints, the scale relationships reporting Joule losses at the modular SRM system are formulated and thereby indicated by (37) and (38). Observing **Figure 6B** it can be concluded that the relative losses increase, as the number of modules increase. That increase is steeper for lower rated powers:

$$P_{JmT} \propto n^{5/9} P_N^{4/9} \quad (37)$$

$$P_{Jr} \propto n^{5/9} P_N^{-5/9} \quad (38)$$

3. Machine design

According to the scale criteria, the previous evaluation of the copper weight and copper losses clearly support the preference for a monolithic topology, instead of a multi-machine topology. The selection of a magnetic structure that considers a shorter flux-path may reduce the magnetomotive force (MMF) absorbed in the iron core.

3.1 Short flux-path topology

Examples of a long flux-path of the regular SRG is presented in **Figure 7A**, and of a short flux-path is presented in **Figure 7B**, highlighting the flux-path closing between two adjacent rotor poles. In order to compare the flux-path length l_{Fsf} of a short flux-path (SFP) topology with the length of the regular machine l_F , an external radius R_2 , similar for both topologies, is considered. The circular arc length of the shaft contour is neglected, for simplicity of analysis. Using the scale laws, it is possible to evaluate the effect on copper losses and weight, in relative terms. The relationship of the flux-paths is given by (39):

$$\frac{l_{Fsf}}{l_F} \cong \frac{\frac{\pi}{m}(R_1 + R_2) + 2(R_2 - R_1)}{\pi R_2 + 2R_2} \quad (39)$$

As inferred from the geometry of both topologies, in the short flux-path case, it is considered a relationship between the exterior and interior radius R_1 given by $R_2 = 3R_1$. Both machines have four phases ($m' = m = 4$), but the SFP topology has a higher number of rotor poles than the reference machine, $N'_R = 14$. With the above assumptions, the ratio of flux-path lengths l_{Fsf}/l_F is approximately 1/2.

Choosing a modular SFP topology, as a magnetic structure, with eight stator modules separated by nonmagnetic spacers, part of the coil wound on the base of each module is exposed, making the copper cooling process and the heat removal more effective. Other favorable arguments to choose this SFP topology are the high fault tolerance, the easy maintenance, and the simplicity of the manufacturing [12].

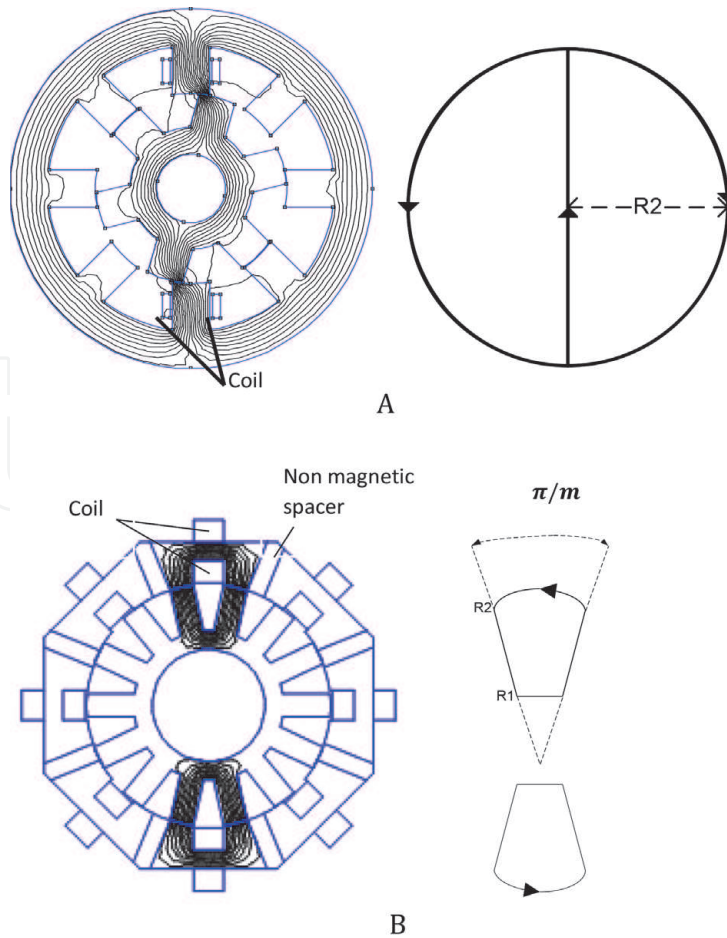


Figure 7. (A) Long flux-path for a regular topology ($m = 4$; $N_R=6$). (B) Short flux-path for a SFP topology ($m = 4$; $N'_R=14$) with stator modules separated by nonmagnetic spacers [1].

The laws related to differentiated scales for copper and iron allow to track the course of the copper losses of the SFP topology, with respect to the regular 8/6 topology. With a limited increase of temperature and a constant flux density, the relationship between the iron and copper characteristic dimensions is expressed by (40) and the copper losses by (41).

$$Bl_F \propto l_{Cu}^{3/2} \quad (40)$$

$$P_J \propto mJ^2 l_{Cu}^3 \propto m l_{Cu}^2 \propto m (Bl_F)^{4/3} \quad (41)$$

The copper losses depend on the length of the flux path, becoming lower in the SFP topology. For identical rated power, the copper losses decrease, considering a wide power range suggests a rescaling operation, i.e., a reduction of the dimensions of the SFP machine compared to the dimensions of the regular machine. For that purpose, together with scale laws, a lumped-parameters model based on field theory will be developed. Previously, in order to build the lumped-parameters model as simple as possible, a finite element analysis is used to evaluate some starting hypothesis. In **Figure 8B** it can be seen that the mutual flux-linkage is very small compared with the flux-linkage of each phase. Therefore, in a similar way to regular topologies, the mutual flux-linkage between two phase windings of the SFP magnetic topology is negligible. The magnetic saturation has a significant effect in this modular SFP topology, as can be seen in **Figure 8A**. However, a steep saturation can also appear in regular machines as it is presented in [13].

3.2 Field-based model for dimensional analysis

Under the scope of scale comparisons and regarding electromagnetic rotating systems, it is suitable to work with simple models representing the distribution of the flux density and the magnetic energy. The torque and power relationships can be estimated with those field-based models, which are supported in real system dimensions. An evaluation of relevant topology characteristics and parameters is expected to be achieved making use of scale laws. Thus, a model of a basic reluctance rotating system will be developed. The core is built with identical and isotopic material, assuming very high magnetic permeability and magnetic linear behavior.

The idea of constructing field-based models, assuming linearity of the magnetic circuit, in such SRG topologies, which are characterized by operating into the

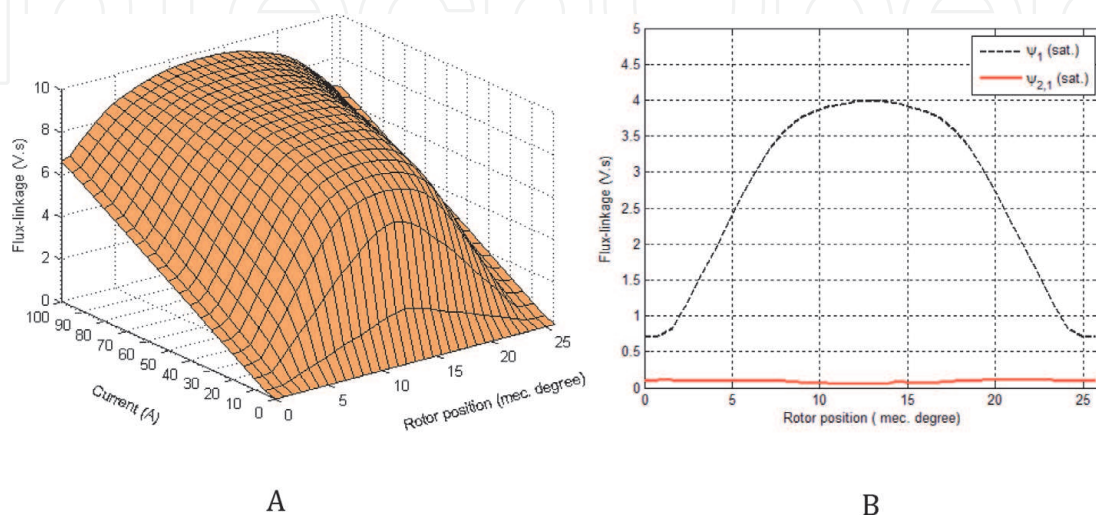


Figure 8.
 (A) Flux-linkage characteristic for the SFP topology. (B) Mutual flux-linkage effect when SFP topology was driven hard into saturation.

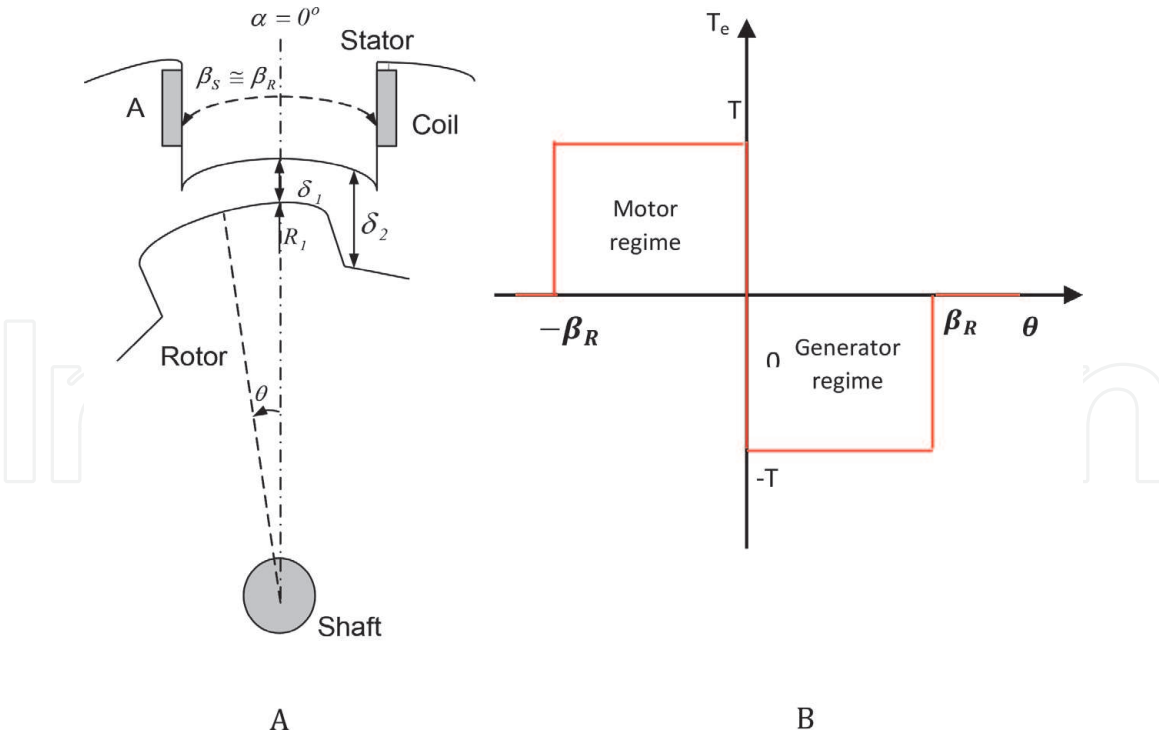


Figure 9. (A) Schematic view of part (two poles) of a basic reluctance rotating system [1]. (B) Torque-position profile and operation regimes of the switched reluctance system [1].

saturation region, may seem contradictory. However, the saturation effect being extended to both topologies, it is possible to compare the characteristics (e.g., having different numbers of poles), preserving certain dimensions of the magnetic circuit where the flux paths lie on. Therefore, the stator external diameter; the air gap length, δ_1 ; the radius of the air gap, R_g ; as well as the core length, L , will be fixed and kept constant.

A part of a basic rotating reluctance system is shown in **Figure 9A**. It is composed of two poles of equal dimensions, one (rotor pole) having the capability of movement with respect to the other (stator pole) which is in a fixed position. One of these poles is confined to an area A and magnetized by a coil with current density J . Thus, a torque will be produced in order to reduce the reluctance of the system magnetic circuit, i.e., by varying the relative position of the poles.

Two angular coordinates are sufficient to determine the position of the rotor pole and the quantities involved in the system. One is the absolute coordinate associated to the inertial fixed referential, α . The other is the coordinate that indicates the relative position of the rotor pole regarding the stator pole, θ . The pole arcs of the rotor and the stator, β_R and β_S , respectively, are approximately equal. It is also assumed that the stator winding comprises another coil, wound on a pole diametrically opposed to the first one, through which the flux-path closes by itself. A last assumption to mention is that the fringing and leakage fields in the air gap will be neglected.

Applying Eq. (1) to this reluctance system yields Eq. (42). Thus, the flux density, B , at the air gap and the magnetic energy stored in the system, W_δ , are expressed by (43) and (44).

$$H_{(\alpha,\theta)} \delta_{(\alpha,\theta)} = JA \quad (42)$$

$$B_{(\alpha,\theta)} = \frac{\mu_o JA}{\delta_{(\alpha,\theta)}} \quad (43)$$

$$W_{\delta} = 2 \int_{V_{\delta}} \left(\int_0^B H \cdot dB' \right) dV = \int_{V_{\delta}} \frac{B^2}{\mu_0} dV \quad (44)$$

It should be noted that (44) includes the presence of two volumes of air gap V_{δ} in the magnetic circuit. Regarding the air gap lengths, it is assumed that $\delta_1 \ll \delta_2$. In these terms, the electromagnetic torque T_e is given by the derivative of the magnetic coenergy W_C with respect to the rotor position (45), and the maximum torque is given by (46). The electromagnetic power, in the generator regime, as well as in the motor regime, shown in **Figure 9B**, is calculated using the average torque $\langle T_e \rangle$ as presented in (47).

$$T_e = \frac{\partial W_C(J, \theta)}{\partial \theta} = \frac{\partial W_{\delta}(J, \theta)}{\partial \theta} \quad (45)$$

$$T = \mu_o (JA)^2 L R_g \left(\frac{1}{\delta_1} - \frac{1}{\delta_2} \right) \cong \frac{\mu_o (JA)^2 L R_g}{\delta_1} \quad (46)$$

$$P = \langle T_e \rangle \omega = m \frac{\beta_R}{\tau_R} \left(\frac{\mu_o A^2 L R_g}{\delta_1} \right) \omega J_{rms}^2 \quad (47)$$

4. Design study results and discussion

The scale law methodology and the field models are used now to compare the SFP topology, represented in **Figure 10A**, with a 12/16 laboratory prototype (three-phase with regular structure), built by M. A. Mueller for a direct drive wind turbine (**Figure 10B**). This topology, with 12 stator and 16 rotor poles, was elected based on torque density criteria [11]. However, the only relevance of that work for the present study lies on the similar parameters of the prototype that will support the scale comparison of topologies. Both magnetic circuits have four stator poles involved in the flux-path when one phase is excited. Identical air gap dimensions and core length (δ, R_g, L) are assumed, and an equal MMF per stator pole is imposed.

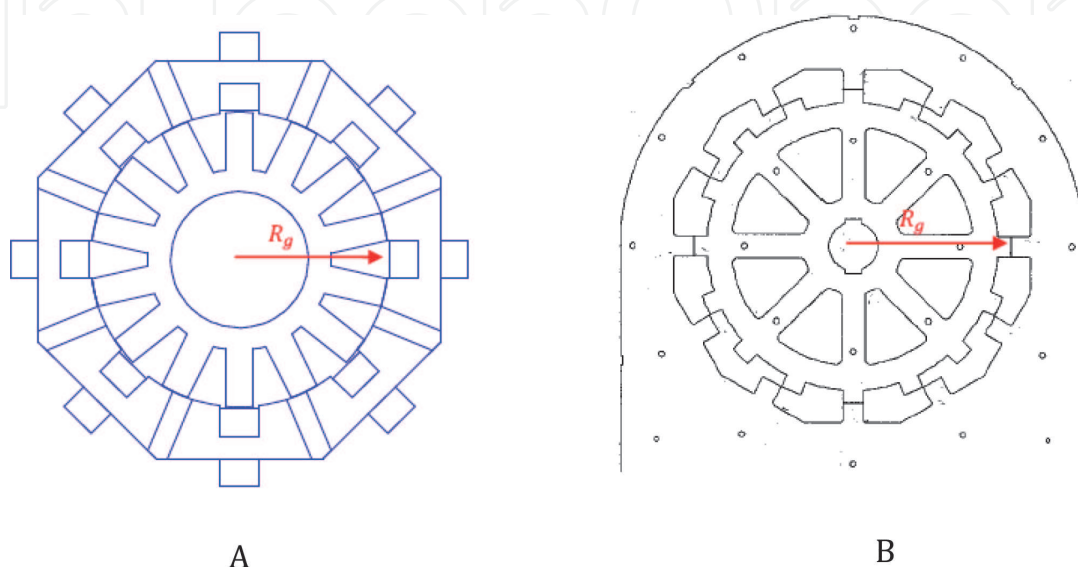


Figure 10.
 (A) Modular SFP topology with identical airgap radius, R_g . (B) SRG prototype (three phases, 12/16).

Thus, Eq. (48) can be used. Concerning the obtained results, the modular SFP topology presents a torque 56% higher than the regular machine. This is an added value that lies on a greater number of phases, m (one more than the prototype) and a larger section of rotor poles, β_R (pole arc of the rotor), as observed in **Table 1**, where the rotor pole pitch is given by $\tau_R = \frac{2\pi}{N_R}$.

The results, in terms of power, allow enough flexibility to perform a rescaling operation of the modular magnetic structure.

Adopting differentiated scales and keeping constant the flux density and the temperature variation, the rated power is expressed by the relationship (48). As illustrated in the diagram of **Figure 11**, and keeping in mind a modular machine and a standard one with equal power ($P'_N = P_N$) to the standard machine (P_N), the proportion of power values presented in **Table 1** enables to infer the following rescaling relationships, (49) and (50):

$$P_N \propto m N_R \omega B^2 l_F^3 \quad (48)$$

$$\frac{P'_N}{P_N} \propto \frac{m' N_R'}{m N_R} \left(\frac{l_F'}{l_F} \right)^3 \quad (49)$$

$$l_F' \propto \left(\frac{1}{1,56} \frac{m N_R}{m' N_R'} \right)^{1/3} l_F \propto 0,82 l_F \quad (50)$$

The rescaling operation shown in **Figure 11** consists on the reduction for identical rated power, in proportional terms, of the modular machine (M_{MOD})

	m	N_R	τ_R [rad]	β_R [rad]	P (p.u)
Regular 12/16 prototype	3	16	$\pi/8$	$\pi/24$	1
SFP modular topology	4	14	$\pi/7$	$\pi/18$	1,56

Table 1.

Parameters of the compared topologies (the base power is peak power), m (number of phases), N_R (number of rotor poles), τ_R (rotor pole-pitch), β_R (rotor pole-arc), P (rated power).

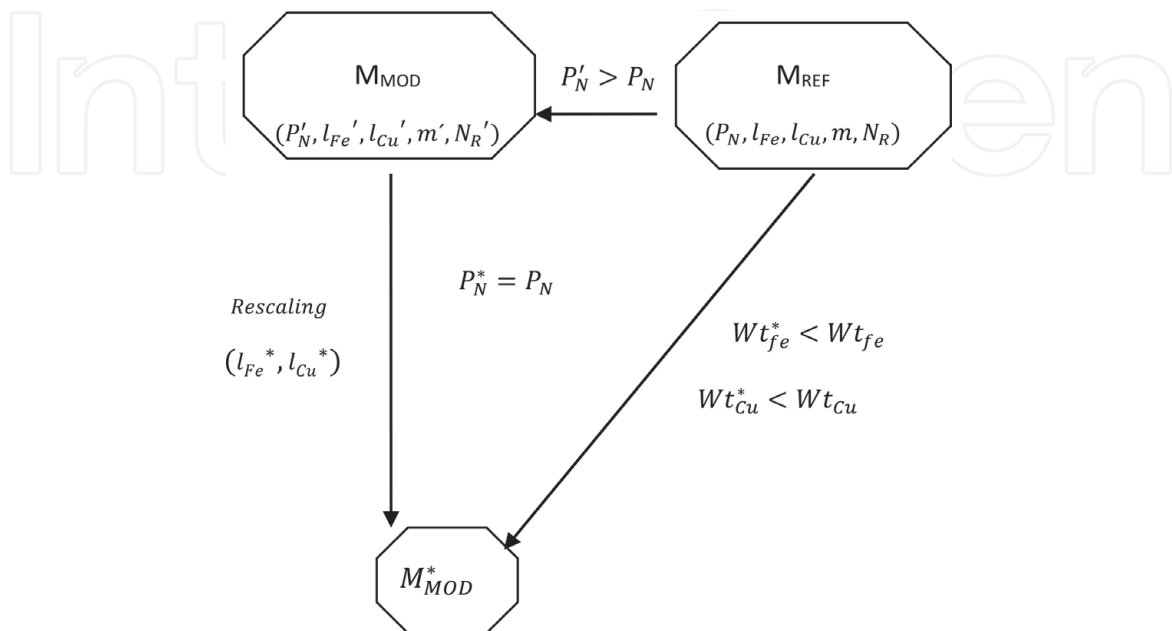


Figure 11.

Schematic diagram of the rescaling operation for weight and loss comparison purposes [1].

characteristic dimensions compared to the standard machine (M_{REF}). After rescaling, it is well-timed to establish relationships for both the weight of iron Wt_F^* and the weight of copper Wt_{Cu}^* as well as to evaluate the copper losses P_{Jr}^* , in relative terms. The iron weight and the copper weight of the modular topology are compared with the SRG prototype, as indicated by (51) and (52):

$$Wt_F^* \propto \frac{(l_F^*)^3}{(l_F)^3} t \propto 0,55 Wt_F \quad (51)$$

$$Wt_{Cu}^* \propto \frac{(l_{Cu}^*)^3}{(l_{Cu})^3} Wt_{Cu} \propto \frac{(l_F^*)^2}{(l_F)^2} Wt_{Cu} \propto 0,67 Wt_{Cu} \quad (52)$$

Regarding the modular topology, the iron weight is approximately 55% when compared to the standard topology, reducing the volume taken by the iron by 45%. Concerning the relative weight of the copper, it allows a reduction of 33% in respect to the regular 12/16 SRG.

In terms of specific power, expressed in W/Kg, it is predicted that there will be an increase of power of 80% at the modular SRG per unit of iron mass, and an increase of close to 50% per unit of copper mass, when compared to the standard SRG. According to the relationships (53) and (54), the relative losses of both machines show the same proportionality, even after the rescaling operation and the resultant reduction of the volume of the modular machine. The rescaling operation is performed on an identical rated power basis:

$$\frac{P_{Jr}^*}{P_{Jr}} = \frac{\frac{P_J^*}{P_N^*}}{\frac{P_J}{P_N}} \propto \frac{m^* (l_{Cu}^*)^2}{m l_{Cu}^2} \propto 1, P_N^* = P_N \quad (53)$$

$$P_{Jr}^* \propto P_{Jr} \quad (54)$$

The weight of the materials is an important factor in choosing the equipment to be used in a generator, due to the general high-altitude location of the wind turbines, whether onshore or offshore. Also, the cost of material and maintenance comes lower, together with lesser weight. Furthermore, when the modular topology is selected, higher fault tolerance is expected. The heat removal and the temperature distributed within the machine take benefit from the modular configuration and the winding location on the stator modules. In fact, the heat transfer is at least so relevant as the electromagnetic design and therefore will be treated in a future work.

Finally, the good performance is preserved, and it is not expected that the inclusion of iron losses in the previous calculations will degrade the results in a significant way.

5. Conclusions

A comparative analysis based on scale models has been presented for low-speed SRM. The comparison and evaluation of magnetic structures play an important role in the SRM design. General design methodologies are usually oriented towards the evaluation of stator/rotor poles combinations for regular SRM. Besides covering that feature, the proposed formulation of scale laws is also suitable to compare other SRM topologies, distinguished by different characteristics of electric and magnetic circuits and their own relative location. As shown by the authors, this methodology

can be extended to other physical phenomena, like thermal changes and magnetic saturation, by introducing some constraints. The study performed in this paper compares a modular short flux-path topology versus a low-speed 20kW prototype SRG, at a rated speed in the region of 100 rpm, designed for a direct drive wind turbine. The modular topology can optimize the efficiency and weight, taking benefits from the significant gain of power per unit of mass and lower losses.

The comparison results achieved in this dimensional analysis indicate that additional work should be developed concerning a detailed design of the modular SFP topology, and so, the work should be seen as a guideline, and not as an end. Considering the real dimensions and the material characteristics, a full-scale machine design will be able to compare initial costs of the modular SFP SRG topology with classical generators, using gearbox.

This work should not be seen as attempting to address a detailed design of a novel SRG, nor an original methodology, but rather highlight the usefulness and effectiveness of the similarity law formulation, as an assistant tool for the machine design. Furthermore, its application to regular and non-regular SRM topologies clearly emphasizes some design details of magnetic structures in machine.

Acknowledgements

The authors thank the Polytechnic Institute of Setúbal and FCT/Nova University of Lisbon for providing facilities as part of an existing cooperation protocol. This work was supported by national funds through FCT under contract UID/EEA/00066/2019.

Author details


Pedro Lobato^{1*}, Joaquim A. Dente² and Armando J. Pires¹

¹ ESTSetúbal, Polytechnic Institute of Setúbal, Setúbal, Portugal

² Instituto Superior Técnico, University of Lisbon, Lisbon, Portugal

*Address all correspondence to: pedro.lobato@estsetubal.ips.pt

IntechOpen

© 2020 The Author(s). Licensee IntechOpen. Distributed under the terms of the Creative Commons Attribution - NonCommercial 4.0 License (<https://creativecommons.org/licenses/by-nc/4.0/>), which permits use, distribution and reproduction for non-commercial purposes, provided the original is properly cited. 

References

- [1] Lobato P, Martins J, Dente JA, Pires AJ. Scale models formulation of switched reluctance generators for low speed energy converters. *IET Electric Power Applications*. 2015;9(9):652-659
- [2] Kioskeridis I, Mademlis C. Optimal efficiency control of switched reluctance generators. *IEEE Transactions on Power Electronics*. 2006;21(4):1062-1071
- [3] Bilgin B, Emadi A, Krishnamurthy M. Design considerations for switched reluctance machines with a higher number of rotor poles. *IEEE Transactions on Industrial Electronics*. 2012;59(10):3745-3756
- [4] Chancharoensook P, Rahman MF. Control of a four-phase switched reluctance generator: experimental investigations. *Proceedings of the IEEE International Electric Machines and Drives Conference*. 2003;2:842-848
- [5] Miller TJE. *Switched Reluctance Motors and Their Control*. Oxford, UK: Magna Physics Publishing and Clarendon Press; 1993
- [6] Bao YJ, Cheng KWE, Cheung NC, Ho SL. Experimental examination on a new switched reluctance wind power generator system for electric vehicles. *IET Power Electronics*. 2012;5(8):1262-1269
- [7] Mueller MA. Design and performance of a 20 kW, 100 rpm, switched reluctance generator for a direct drive wind energy converter. In: *Proceedings of the IEEE International Conference on Electric Machines and Drives*. San Antonio, Texas, U.S.A.; 2005. pp. 56-63
- [8] Jufer M. *Electric Drive: Design Methodology*. UK: ISTE Ltd and John Wiley & Sons Inc; 2010
- [9] Boldea I, Tutelea L, Blaabjerg F. High power wind generator designs with less or no PMs: An overview. In: *Proceedings of 17th International Conference on Electrical Machines and Systems (ICEMS)*. Hangzhou, China; 2014
- [10] Liu X, Park K, Chen Z. A novel excitation assistance switched reluctance wind power generator. *IEEE Transactions on Magnetics*. 2014; 50(11):1-4
- [11] Mueller MA. Design and performance of a 20 kW, 100 rpm, switched reluctance generator for a direct drive wind energy converter. In: *Proceedings of the IEEE International Conference on Electric Machines and Drives*. San Antonio, Texas, U.S.A.; 2005. pp. 56-63
- [12] Ruba M, Viorel I, Szabó L. Modular stator switched reluctance motor for fault tolerant drive systems. *IET Electric Power Applications*. 2013;7(3):159-169
- [13] Parreira B, Rafael S, Pires AJ, Costa Branco PJ. Obtaining the magnetic characteristics of an 8/6 switched reluctance machine: FEM analysis and experimental tests. *IEEE Transactions on Industrial Electronics*. 2005;52(6):1635-1643